

Scaling of disorder operator at deconfined quantum criticality

Yan-Cheng Wang,¹ Nvsn Ma,² Meng Cheng,^{3,*} and Zi Yang Meng^{4,†}

¹*School of Materials Science and Physics, China University of Mining and Technology, Xuzhou 221116, China*

²*School of Physics, Key Laboratory of Micro-Nano Measurement-Manipulation and Physics, Beihang University, Beijing 100191, China*

³*Department of Physics, Yale University, New Haven, CT 06520-8120, U.S.A*

⁴*Department of Physics and HKU-UCAS Joint Institute of Theoretical and Computational Physics, The University of Hong Kong, Pokfulam Road, Hong Kong SAR, China*

(Dated: May 5, 2022)

We study the scaling behavior of the disorder parameter, defined as the expectation value of a symmetry transformation applied to a finite region, at the deconfined quantum critical point in $(2+1)d$ in the $J-Q_3$ model via large-scale quantum Monte Carlo simulations. We show that the disorder parameter for $U(1)$ spin rotation symmetry exhibits perimeter scaling with a logarithmic correction associated with sharp corners of the region, as generally expected for a conformally-invariant critical point. However, for large rotation angle the universal coefficient of the logarithmic corner correction becomes negative, which is not allowed in any unitary conformal field theory. We also extract the current central charge from the small rotation angle scaling, whose value is much smaller than that of the free theory.

Introduction. -Deconfined quantum criticality (DQC) [1–3], a continuous quantum phase transition between two seemingly unrelated symmetry-breaking states, is arguably the enigma of novel quantum critical point beyond the paradigm of Landau-Ginzburg-Wilson. Such a transition, if exists, is believed to host a number of unusual phenomena, such as an emergent symmetry unifying order parameters of completely different microscopic origins and the presence of fractionalized spinons, among others [3–5]. Theoretically the proposed low-energy theory is a gauge theory in the strong coupling regime, posing significant challenges to analytical treatment [2, 6]. Numerical investigations of lattice models realizing such transitions have been indispensable in pushing forward our understanding of DQC from many different angles: the two-length-scale scaling as an attempt to reconcile the anomalous finite-size scaling behavior of the $J-Q$ model [7], conserved current exploited to exhibit the emergent continuous symmetry [8], fractionalization revealed from dynamic spin spectra [3], to name a few. There has also been exciting progress in possible experimental realization of the DQC from the pressure-driven phase transition in the Shastry-Sutherland quantum magnet $\text{SrCu}_2(\text{BO}_3)_2$ [9, 10] and its theoretical implications [11–13]. The communities of quantum phase transitions, quantum magnetism and even high-energy physics, have benefited a lot from these pursuits over the years. However, the very nature of the transition itself, and basic questions such as whether the transition is continuous or not, whether the transition follows conformal invariance and acquires a proper conformal field theory (CFT) description [6, 14–17], etc, are actually still open despite the active investigations mentioned above.

In recent years, the importance of using extended operators, such as symmetry domain walls or field lines of emergent gauge field, to probe and characterize phases and phase transitions has become increasingly clear [18–22]. In particular, many exotic gapped phases can be understood in terms of the condensation of certain extended objects, spontaneously breaking the so-called higher-form symmetry. These new insights bring intriguing connections between the Landau-

Ginzburg-Wilson paradigm of spontaneous symmetry breaking and more exotic phenomena of topological order [23]. Inspired by such progress, recent works have started to explore more quantitative aspects of disorder operators, which is defined as a symmetry transformation restricted to a finite region of the system, especially at quantum criticality. Ref. [24] computed the Ising disorder operator, which serves as the order parameter of a \mathbb{Z}_2 1-form symmetry, by quantum Monte Carlo (QMC) simulation at the $(2+1)d$ Ising transition. $U(1)$ disorder operator at the $(2+1)d$ XY transition is measured in QMC simulation as well [25]. New universal scaling behavior for such disorder operators at these conformally-invariant quantum critical points (QCP) are identified. Building upon the methodology for the computation and analysis of disorder operator established by studying conventional symmetry-breaking transitions, in this work we take this new set of tools to study the deconfined quantum criticality.

An important difference between the DQC and other QCPs studied so far in this context is that one side of DQC exhibits the Valence Bond Solid (VBS) order, spontaneously breaking the lattice symmetry. To understand how the behavior of disorder operator is affected by lattice symmetry breaking, we first study two different microscopic realizations of the $(2+1)$ $O(3)$ QCP, the bilayer and J_1 - J_2 Heisenberg antiferromagnets on square lattice, using QMC simulations. We find the disorder operators for $U(1)_{S_z}$ symmetry obey the expected perimeter law scaling with a multiplicative logarithmic correction at the QCPs, in agreement with the prediction of the $O(3)$ CFT. However for the J_1 - J_2 model with explicit translation symmetry breaking, it is crucial to construct disorder operators only on regions whose boundary avoids the “strong” singlet bonds, in order to obtain converged results in the finite-size analysis.

With this knowledge, we proceed with the similar measurement of the $U(1)_{S_z}$ disorder operator in the $J-Q_3$ model of DQC, at the critical point between the Néel and VBS phases [4]. To have controlled results, we employ a small pinning field of the VBS order and follow the same prescription for the construction of disorder operator established in

the study of the J_1 - J_2 model. Our converged data reveal that although the disorder operator still obeys the scaling behavior expected for a general CFT, the universal coefficient in the logarithmic correction term becomes negative for U(1) rotation angle close to π , which we argue is incompatible with any unitary CFT. We also extract the current central charge from the small angle scaling, whose value is significantly smaller than conventional $O(n)$ CFT.

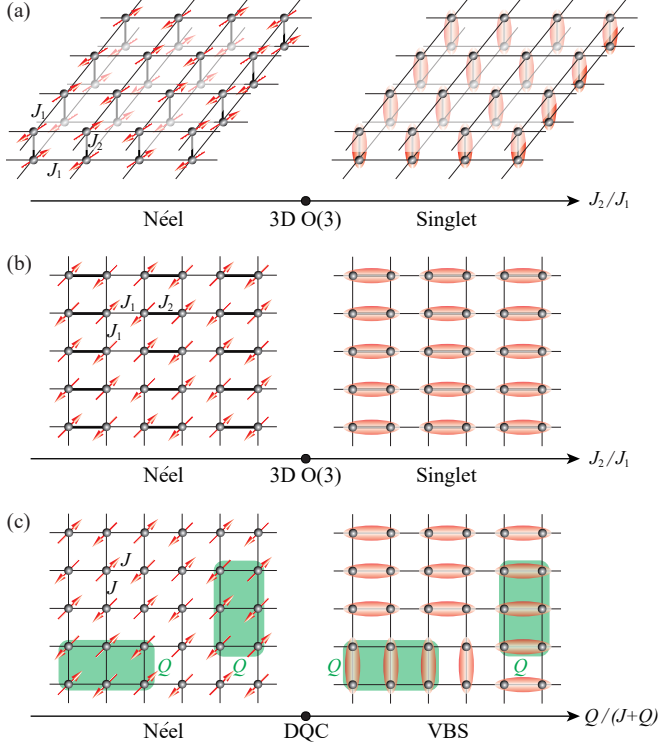


FIG. 1. The three lattice models: (a) the bilayer square lattice antiferromagnetic Heisenberg model, (b) the square lattice J_1 - J_2 antiferromagnetic Heisenberg model and (c) the J - Q_3 model. (a), (b) exhibits $(2+1)d$ $O(3)$ QCP as J_2/J_1 is tuned [26–28] and (c) gives rise to DQC [4].

Three lattice models.— We simulate the following three lattice models hosting the target QCPs. The first is the bilayer square lattice antiferromagnet with Hamiltonian

$$H_{\text{bilayer}} = J_1 \sum_{\langle ij \rangle} (\mathbf{S}_{1,i} \cdot \mathbf{S}_{1,j} + \mathbf{S}_{2,i} \cdot \mathbf{S}_{2,j}) + J_2 \sum_i \mathbf{S}_{1,i} \cdot \mathbf{S}_{2,i}, \quad (1)$$

where $\mathbf{S}_{\alpha,i}$ is a spin-1/2 at site i of layer $\alpha (= 1, 2)$, $\langle ij \rangle$ denotes the nearest-neighbor antiferromagnetic coupling on the square lattice. J_2 is the interlayer antiferromagnetic interaction. The model is illustrated in Fig. 1(a). The critical point $(J_2/J_1)_c = 2.5220(1)$ [26, 27] separating the Néel state and the symmetric product state of inter-layer singlets, belongs to the $(2+1)d$ $O(3)$ universality class.

The next model is the square lattice J_1 - J_2 Heisenberg, shown in Fig. 1(b). The Hamiltonian reads

$$H_{J_1-J_2} = J_1 \sum_{\langle ij \rangle} \mathbf{S}_i \cdot \mathbf{S}_j + J_2 \sum_{\langle ij \rangle'} \mathbf{S}_i \cdot \mathbf{S}_j, \quad (2)$$

where $\langle ij \rangle$ denotes the thin J_1 bond and $\langle ij \rangle'$ denotes the thick J_2 bond, and the QCP $(J_2/J_1)_c = 1.90951(1)$ [28] is also known to fall within the $(2+1)d$ $O(3)$ universality class. The reason that we study both Eqs. (1) and (2) is that although the QCPs are in the same universality class, the presence of strong J_2 and weak J_1 bonds in Eq. (2) breaks the lattice translation symmetry while Eq. (1) is fully translation-invariant. As we show below, because of the translation symmetry breaking, the domain M must be chosen so that its boundary avoids strong singlet bonds to correctly extract the scaling behavior of the disorder operator.

The last model is the J - Q_3 model as illustrated in Fig. 1(c) with the following Hamiltonian,

$$H_{J-Q_3} = -J \sum_{\langle ij \rangle} P_{ij} - Q \sum_{\langle ijklmn \rangle} P_{ij} P_{kl} P_{mn}. \quad (3)$$

Here $P_{ij} = \frac{1}{4} - \mathbf{S}_i \cdot \mathbf{S}_j$ is the two-spin singlet projector. The quantum critical point separating the Néel and VBS states is at $[Q/(J+Q)]_c = 0.59864(4)$ [4, 7]. While the VBS order vanishes at the QCP after extrapolating to the thermodynamic limit, in a finite system there is always a small but non-zero VBS order. Therefore the computation of the disorder parameter may suffer from similar kinds of lattice effect that occurs in the J_1 - J_2 model. To eliminate such effect as much as possible, we follow the same procedure used to extract the universal scaling for the disorder parameter in the J_1 - J_2 case, to achieve robustly converged results from finite-size analysis.

Disorder operator.— All three lattice models have $SU(2)$ spin rotational symmetry. For any U(1) subgroup we will define a disorder operator that depends on the U(1) rotation angle. Without loss of generality, we will consider spin rotations around the z and the U(1) symmetry transformations are implemented by $U(\theta) = \prod_i e^{i\theta(S_i^z - \frac{1}{2})}$, where S_i^z is the U(1) charge on site i . For a region M , we define the disorder operator $X_M(\theta) = \prod_{i \in M} e^{i\theta(S_i^z - \frac{1}{2})}$. The ground state expectation value $\langle X_M(\theta) \rangle$ will be referred to as the disorder parameter. The scaling behavior of $\langle X_M(\theta) \rangle$ in various phases, especially the dependence on the geometry of M , has been studied thoroughly in Ref. [25]. In a U(1)-symmetric phase, such as the singlet ground state in H_{bilayer} and $H_{J_1-J_2}$ models, $\langle X_M(\theta) \rangle$ is expected to obey a perimeter law $|\langle X_M(\theta) \rangle| \sim e^{-a_1(\theta)l}$, where l is the perimeter of the region M . In the ordered (U(1) symmetry breaking) phases, such as the Néel phase of the three models, it was found that $|\langle X_M(\theta) \rangle| \sim e^{-b(\theta)l \ln l}$ [25, 29]. Our focus in this work, however, is the disorder operator at QCPs in Fig. 1, in particular that of the DQC. Previous studies of the $(2+1)d$ Ising and $O(2)$ transitions, as well as other gapless critical theories [24, 25, 30, 31] suggest that $\ln |\langle X_M(\theta) \rangle|$ takes the following general form for a rectangle region:

$$\ln |\langle X_M(\theta) \rangle| = -a_1 l + s \ln l + a_0. \quad (4)$$

Here all the coefficients are functions of θ . The universal logarithmic correction, which translates into a power law l^s in $|\langle X_M \rangle|$, originates from sharp corners of the region. In general s is a universal function of both θ and the opening angle(s) of

the corners (all $\pi/2$ in this case) [25, 32]. Similar corner contributions are known to arise for Rényi entropy in a CFT [33], which can be understood as the disorder operator of the replica symmetry. In Ref. [25], analytical arguments were presented to support the universal corner correction for the disorder operator and the universal coefficient s is found to be given by $s(\theta) \approx \frac{C_J}{(4\pi)^2} \theta^2$ as $\theta \rightarrow 0$ (see also Ref. [31]). Here C_J is the current central charge of the CFT, which is proportional to the universal DC conductivity $\sigma = \frac{\pi}{16} C_J$ [34]. This is the consequence of conformal symmetry and current conservation. Our previous QMC at O(2) QCP reveals $s/\theta^2 = 0.011(1)$, consistent with the exact value $\frac{C_J}{(4\pi)^2} = 0.01145$ [35–38]. Another feature common to all known examples of disorder operators is that s is always positive. The positivity of s is proven for the Rényi entropy, i.e. disorder parameter of the replica symmetry in unitary CFTs [39, 40]. In the present case, we generalize the argument in Ref. [39] to show that $s(\pi)$ must be positive in a unitary CFT (see Supplemental Materials (SM) for details). As we will see below, $s(\theta)$ for DQC follows the same scaling behavior at small θ , but the large θ behavior is dramatically different.

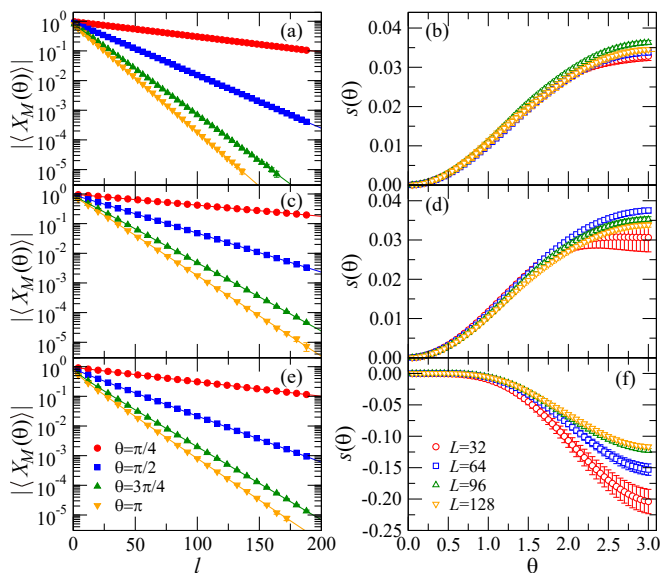


FIG. 2. Disorder parameter $|\langle X_M(\theta) \rangle|$ as a function of the perimeter $l = 4R - 4$ with system size $L = 96$ at the QCPs for H_{bilayer} model (a), $H_{J_1-J_2}$ model (c) and the H_{J-Q_3} model (e). In (e), a small pinning field $J_2 = J + \frac{\delta}{L}$ with $\delta = 0.05$ is applied to pin the VBS order, in order to have well-converged results for the disorder operator (see the analysis in the text). (b), (d) and (f) show the obtained $s(\theta)$ with system size $L = 32, 64, 96, 128$ for the three models in (a), (c) and (e), respectively. The convergence of the data with increasing L is clear from the figures.

Numerical Results. - We choose the region M to be a $R \times R$ square region in the lattice, with perimeter $l = 4R - 4$. Firstly, we compute the disorder parameter $X_M(\theta)$ as a function of perimeter l at the 3D O(3) QCP ($(J_2/J_1)_c = 2.5220$) [26, 27] of the H_{bilayer} model with system size $L = 32, 64, 96, 128$. Plots of $|\langle X_M(\theta) \rangle|$ v.s. l for representative values of θ 's are

shown in Fig. 2(a). Fitting the data with Eq. (4), we obtain the coefficient $s(\theta)$ of the corner correction term, as shown in Fig. 2 (b). The behavior of s is qualitatively similar to that of the O(2) transition studied in Ref. [25]. We will mainly use the results from H_{bilayer} as a reference for the O(3) CFT.

Next, we perform the same QMC simulations for the $H_{J_1-J_2}$ model at its QCP $(J_2/J_1)_c = 1.90951(1)$ [28]. Although the critical theory is the same 3D O(3) CFT, because of the doubling of the unit cell due to alternating J_1 and J_2 bonds, the disorder parameter $\langle X_M(\theta) \rangle$ exhibits even-odd oscillation as a function of R , see SM for details. This is because the boundary of the region M cuts different types of bonds for even and odd R : for odd R , one of the boundary segments along y always cuts strong J_2 bonds, while for even R depending on the exact position of M the boundary may or may not cut strong bonds. Such singlet cutting increases the leading perimeter contribution in the disorder parameter, introducing significant finite-size error when extracting the subleading corner term s . For the J_1-J_2 model, we find that the correct results for $s(\theta)$ (compared to $s(\theta)$ extracted from the bilayer Heisenberg model, free of such complications) can only be obtained from the scaling analysis when disorder operators are constructed on regions whose boundary does not cut any strong bonds. More details of the analysis can be found in the SM. We believe this is a general phenomenon and to mitigate finite-size error similar selection of regions must be applied whenever there exists bond order breaking the translation symmetry either explicitly or spontaneously. This is the most important lesson learnt from the study of the J_1-J_2 model.

Now we turn to the $J-Q_3$ model. Because of the VBS order, we would like to design the boundary of M in such a way that it does not cut any strong singlet bonds. However, since the VBS order in the $J-Q_3$ model forms spontaneously, the pattern of stronger singlet bonds is not known a priori. To resolve this issue, we employ a small pinning field to lock the VBS order into a particular pattern, e.g. the singlet bonds are oriented along the x -direction similar to those in the J_1-J_2 model, as illustrated in Fig. 1 (b). This is achieved by strengthening the Heisenberg couplings on the J_2 bonds. To make sure that the quantum criticality is not spoiled by the explicit breaking of the symmetry, we purposefully choose the strength of the field to scale with $1/L$ with a small coefficient δ , i.e. $J_2 = J + \frac{\delta}{L}$, such that when extrapolating to the thermodynamic limit, the simulated Hamiltonian goes back to the original H_{J-Q_3} with only spontaneous symmetry breaking. We find the value of $\delta = 0.05$ gives the most robust and well-converged results of $\langle X_M \rangle$, as shown in Fig. 2 (e) and (f). Hence all results reported below are obtained with such a pinning field. Similar type of pinning has also been shown to work in other difficult QCPs [41, 42].

Let us start from small θ . In Fig. 3, we show the fit of the corner correction $s(\theta)$ for small $\theta (\leq 0.25)$ with $s(\theta) = \frac{C_J}{(4\pi)^2} \theta^2$. For the H_{bilayer} and $H_{J_1-J_2}$ Heisenberg models, we obtain $C_J/(4\pi)^2 = 0.0120(2)$ and $C_J/(4\pi)^2 = 0.0116(2)$, respectively. These values are consistent with $C_J/(4\pi)^2 = 0.01147$ of the O(3) CFT from numerical bootstrap [43] within er-

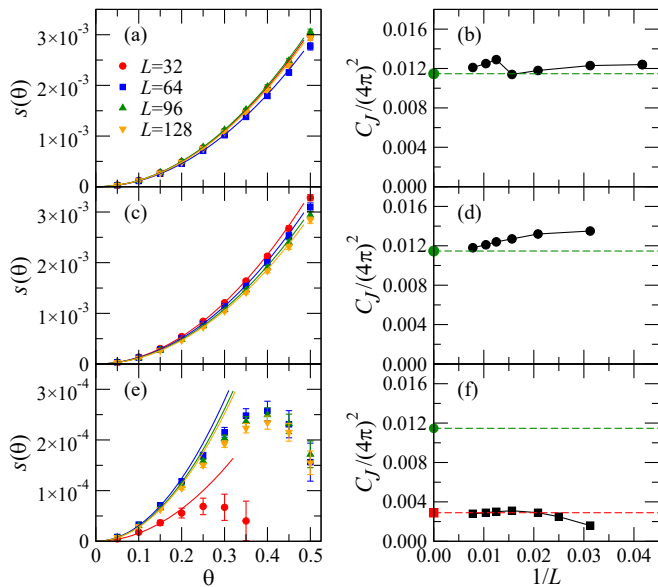


FIG. 3. The coefficient of the corner correction $s(\theta)$ for small values of θ with system size $L = 32, 64, 96, 128$ at the QCPs for H_{bilayer} model (a), $H_{J_1-J_2}$ model (c) and H_{J-Q_3} model (e). The lines are the data fitting with $s(\theta) = \frac{C_J}{(4\pi)^2} \theta^2$. (b), (d) and (f) show the extrapolation of the obtained $C_J/(4\pi)^2$ as the system size L increases. In case of (b) and (d), the extrapolated $C_J/(4\pi)^2$ approach the theoretical value 0.0111 for the $O(3)$ CFT denoted by the green dots and dashe lines. In (f), $C_J/(4\pi)^2$ for DQC apparently extrapolates to a much smaller number (red square and dashed line), around one quarter of the $O(3)$ value (the green dot and dashed line).

rorbars. However, as shown in Fig. 3 (e) and (f), the same analysis for the DQC yields a much smaller value $C_J/(4\pi)^2 = 0.0028(2)$, roughly one quarter of that of the $O(n)$ CFTs. A small C_J , or equivalently a small DC conductivity σ , suggests that the theory is strongly coupled (so the value deviates significantly from that of a free boson).

Most interestingly, we find that the $s(\theta)$ for DQC becomes negative for large θ as shown in Fig. 2 (f). We also note that $s(\theta)$ converges quite well as the system size increases up to $L = 128$. Such negative values of $s(\theta)$ in DQC are drastically different from the behavior of s observed in all other QCPs investigated so far, including Ising [24], $O(2)$ [25] and also the two different realizations of the $O(3)$ CFT in Fig. 2 (b) and (d). This list can be expanded to include Rényi entanglement entropy as a disorder parameter of the replica symmetry, and it is known that the corner correction s for Rényi entropies must be positive for all unitary CFTs [39, 40]. In fact, we can generalize the argument in Ref. [39] to show that $s(\theta = \pi) > 0$ (essentially for any \mathbb{Z}_2 symmetry disorder parameter, see SM for details). Therefore a negative s implies strong deviation of the model from unitary CFTs. This is intriguing as measurements of local observables at DQC in the H_{J-Q_3} model appear to exhibit conformal invariance, at least for system sizes accessible to current numerical simulations. Thus our observation of a negative $s(\pi)$ provides direct evidence for the breakdown

of a unitary CFT description.

Discussions.- Through large-scale QMC simulations and finite-size analyses, we determine the scaling behavior of the disorder operator for $U(1)_{S_z}$ symmetry at the DQCP in the $J-Q_3$ model. Most noticeably, the universal corner correction s of the DQC becomes negative, in sharp contradiction to the positivity of $s(\pi)$ in any unitary relativistic conformal field theory. We also observe that the obtained current central charge of DQC is much smaller than the typical value of $O(n)$ CFTs, suggesting possible fractionalization of the charge carriers at DQC.

Our findings, in particularly the negative s , raise a number of significant questions about the theory of DQC. One possible explanation for the negative s is that the observed regime of the DQC is actually controlled by a non-unitary CFT, with a (complex) fixed point very close to the physical parameter space. So within a large length scale conformal invariance can still manifest. This possibility has been proposed theoretically in several recent works [6, 15–17], to explain unusual finite-size scaling behavior from previous numerical simulations [6, 7, 14] and the tension between the numerically observed critical exponents with conformal bootstrap bounds. Our result points to a distinct aspect of this putative non-unitary fixed point, that the universal correction s must be negative. On the other hand, it is also important to understand how the two-length-scale scaling [7], and theoretically the existence of a dangerously irrelevant operator due to the breaking of the emergent symmetry by lattice effect, affect the behavior of the disorder operator. It will be interesting for future studies to explore other non-local observables, such as Rényi entropies, and consider other microscopic realizations of DQC where dangerously irrelevant operators are absent [44]. In summary, our results unambiguously reveal fundamental differences between DQC and QCPs described by unitary CFTs, shedding new lights on the nature of DQC.

Acknowledgement.- We are grateful to Hui Shao for sharing unpublished data on the $J-Q_3$ model. We would like to thank Cenke Xu, Chao-Ming Jian and Fakher Assaad for comments on a draft. M.C. thanks Yi-Zhuang You for enlightening conversations on DQCP. Y.C.W. acknowledges the supports from the NSFC under Grant No. 11804383 and No. 11975024, the NSF of Jiangsu Province under Grant No. BK20180637, and the Fundamental Research Funds for the Central Universities under Grant No. 2018QNA39. N.M. acknowledges the supports from the NSFC under Grant No. 12004020. M.C. acknowledges support from NSF under award number DMR-1846109 and the Alfred P. Sloan foundation. Z.Y.M. acknowledges support from the RGC of Hong Kong SAR of China (Grant Nos. 17303019, 17301420 and AoE/P-701/20), MOST through the National Key Research and Development Program (Grant No. 2016YFA0300502) and the Strategic Priority Research Program of the Chinese Academy of Sciences (Grant No. XDB33000000). We thank the Computational Initiative at the Faculty of Science and the Information Technology Services at the University of Hong Kong and the Tianhe platforms at the National Supercomputer Centers in Tianjin and

Guangzhou for their technical support and generous allocation of CPU time.

* m.cheng@yale.edu

† zymeng@hku.hk

- [1] A. W. Sandvik, *Phys. Rev. Lett.* **98**, 227202 (2007).
- [2] T. Senthil, L. Balents, S. Sachdev, A. Vishwanath, and M. P. A. Fisher, *Phys. Rev. B* **70**, 144407 (2004).
- [3] N. Ma, G.-Y. Sun, Y.-Z. You, C. Xu, A. Vishwanath, A. W. Sandvik, and Z. Y. Meng, *Phys. Rev. B* **98**, 174421 (2018).
- [4] J. Lou, A. W. Sandvik, and N. Kawashima, *Phys. Rev. B* **80**, 180414 (2009).
- [5] A. Nahum, P. Serna, J. T. Chalker, M. Ortuño, and A. M. Somoza, *Phys. Rev. Lett.* **115**, 267203 (2015).
- [6] C. Wang, A. Nahum, M. A. Metlitski, C. Xu, and T. Senthil, *Phys. Rev. X* **7**, 031051 (2017).
- [7] H. Shao, W. Guo, and A. W. Sandvik, *Science* **352**, 213 (2016).
- [8] N. Ma, Y.-Z. You, and Z. Y. Meng, *Phys. Rev. Lett.* **122**, 175701 (2019).
- [9] J. Guo, G. Sun, B. Zhao, L. Wang, W. Hong, V. A. Sidorov, N. Ma, Q. Wu, S. Li, Z. Y. Meng, A. W. Sandvik, and L. Sun, *Phys. Rev. Lett.* **124**, 206602 (2020).
- [10] J. L. Jiménez, S. P. G. Crone, E. Fogh, M. E. Zayed, R. Lortz, E. Pomjakushina, K. Conder, A. M. Läuchli, L. Weber, S. Wessel, A. Honecker, B. Normand, C. Rüegg, P. Corboz, H. M. Rønnow, and F. Mila, *Nature* **592**, 370 (2021).
- [11] B. Zhao, P. Weinberg, and A. W. Sandvik, *Nature Physics* **15**, 678 (2019).
- [12] G. Sun, N. Ma, B. Zhao, A. W. Sandvik, and Z. Y. Meng, arXiv e-prints, arXiv:2103.00863 (2021), arXiv:2103.00863 [cond-mat.str-el].
- [13] J. Yang, A. W. Sandvik, and L. Wang, arXiv e-prints, arXiv:2104.08887 (2021), arXiv:2104.08887 [cond-mat.str-el].
- [14] A. Nahum, J. T. Chalker, P. Serna, M. Ortuño, and A. M. Somoza, *Phys. Rev. X* **5**, 041048 (2015).
- [15] A. Nahum, *Phys. Rev. B* **102**, 201116 (2020).
- [16] R. Ma and C. Wang, *Phys. Rev. B* **102**, 020407 (2020).
- [17] Z. Wang, M. P. Zaletel, R. S. K. Mong, and F. F. Assaad, *Phys. Rev. Lett.* **126**, 045701 (2021).
- [18] Z. Nussinov and G. Ortiz, *Proc. Nat. Acad. Sci.* **106**, 16944 (2009), arXiv:cond-mat/0605316.
- [19] Z. Nussinov and G. Ortiz, *Annals Phys.* **324**, 977 (2009), arXiv:cond-mat/0702377.
- [20] D. Gaiotto, A. Kapustin, N. Seiberg, and B. Willett, *J. High Energy Phys.* **2015** (2015), 10.1007/jhep02(2015)172, arXiv:1412.5148.
- [21] W. Ji and X.-G. Wen, “Categorical symmetry and non-invertible anomaly in symmetry-breaking and topological phase transitions,” (2019), arXiv:1912.13492.
- [22] L. Kong, T. Lan, X.-G. Wen, Z.-H. Zhang, and H. Zheng, “Algebraic higher symmetry and categorical symmetry – a holographic and entanglement view of symmetry,” (2020), arXiv:2005.14178.
- [23] X.-G. Wen, *Science* **363**, 834 (2019).
- [24] J. Zhao, Z. Yan, M. Cheng, and Z. Y. Meng, arXiv e-prints (2020), arXiv:2011.12543.
- [25] Y.-C. Wang, M. Cheng, and Z. Y. Meng, arXiv e-prints, arXiv:2101.10358 (2021), arXiv:2101.10358 [cond-mat.str-el].
- [26] L. Wang, K. S. D. Beach, and A. W. Sandvik, *Phys. Rev. B* **73**, 014431 (2006).
- [27] M. Lohöfer, T. Coletta, D. G. Joshi, F. F. Assaad, M. Vojta, S. Wessel, and F. Mila, *Phys. Rev. B* **92**, 245137 (2015).
- [28] N. Ma, P. Weinberg, H. Shao, W. Guo, D.-X. Yao, and A. W. Sandvik, *Phys. Rev. Lett.* **121**, 117202 (2018).
- [29] E. Lake, (2018), arXiv:1802.07747.
- [30] X.-C. Wu, W. Ji, and C. Xu, arXiv e-prints (2020), arXiv:2012.03976.
- [31] X.-C. Wu, C.-M. Jian, and C. Xu, arXiv e-prints, arXiv:2101.10342 (2021), arXiv:2101.10342 [cond-mat.str-el].
- [32] B. Estienne, J.-M. Stéphan, and W. Witczak-Krempa, arXiv e-prints, arXiv:2102.06223 (2021), arXiv:2102.06223 [cond-mat.str-el].
- [33] A. B. Kallin, E. M. Stoudenmire, P. Fendley, R. R. P. Singh, and R. G. Melko, *J. Stat. Mech.* **2014**, 06009 (2014), arXiv:1401.3504.
- [34] M. P. A. Fisher, G. Grinstein, and S. M. Girvin, *Phys. Rev. Lett.* **64**, 587 (1990).
- [35] W. Witczak-Krempa, E. S. Sørensen, and S. Sachdev, *Nature Physics* **10**, 361 (2014).
- [36] E. Katz, S. Sachdev, E. S. Sørensen, and W. Witczak-Krempa, *Phys. Rev. B* **90**, 245109 (2014).
- [37] K. Chen, L. Liu, Y. Deng, L. Pollet, and N. Prokof'ev, *Phys. Rev. Lett.* **112**, 030402 (2014).
- [38] S. M. Chester, W. Landry, J. Liu, D. Poland, D. Simmons-Duffin, N. Su, and A. Vichi, *J. High Energy Phys.* **2020** (2020), 10.1007/jhep06(2020)142.
- [39] H. Casini and M. Huerta, *Journal of High Energy Physics* **2012**, 87 (2012).
- [40] P. Bueno, R. C. Myers, and W. Witczak-Krempa, *J. High Energy Phys.* **09**, 091 (2015), arXiv:1507.06997.
- [41] F. F. Assaad and I. F. Herbut, *Phys. Rev. X* **3**, 031010 (2013).
- [42] W. Wang, D.-C. Lu, X. Y. Xu, Y.-Z. You, and Z. Y. Meng, *Phys. Rev. B* **100**, 085123 (2019).
- [43] D. Poland, S. Rychkov, and A. Vichi, *Rev. Mod. Phys.* **91**, 015002 (2019).
- [44] Y. Liu, Z. Wang, T. Sato, M. Hohenadler, C. Wang, W. Guo, and F. F. Assaad, *Nat. Commun.* **10** (2019), 10.1038/s41467-019-10372-0.

SUPPLEMENTAL MATERIAL

The choice of region M

In this section, we discuss how to choose the region M to obtain the correct scaling behavior of $\langle X_M \rangle$. As shown in the main text, for H_{bilayer} , since there is no translation symmetry breaking (explicit or spontaneous), the choice of the region is immaterial. However, the $J_1 - J_2$ case is different because the alternating strengths of Heisenberg couplings doubles the unit cell, as shown in Fig. S4. If the region M is a $R \times R$ square (green shaded region in Fig. S4), M with even or odd R cut very different types of bonds on the boundary.

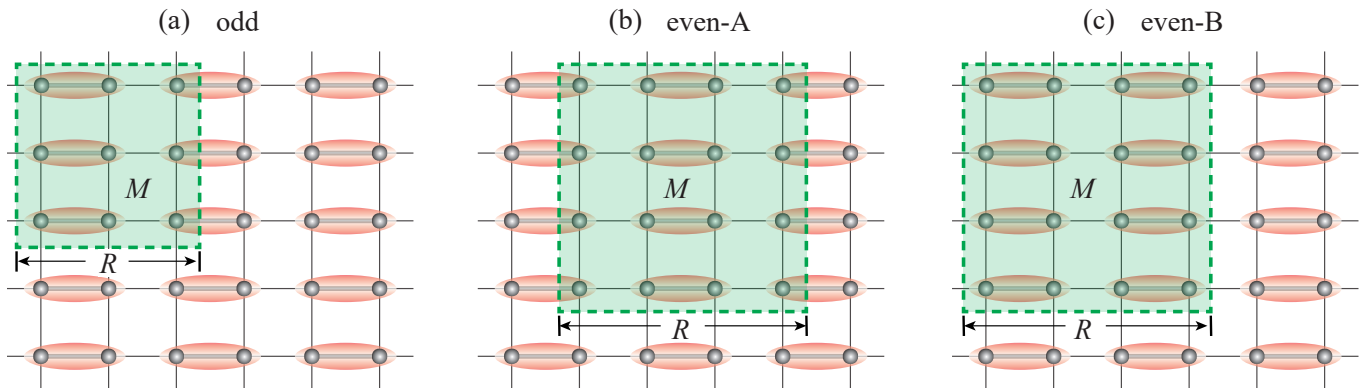


FIG. S4. Three types of region M : (a) region M with odd $R(= 3)$, whose boundary cuts one column of strong singlet bonds; (b) region M with even $R(= 4)$ and cutting two columns of strong singlet bonds; (c) region M with even $R(= 4)$ and cutting no strong singlet bonds.

More concretely, when R is odd (e.g. $R = 3$ in Fig. S4 (a)), the boundary of M inevitably cuts one column of J_2 bonds. When R is even, as shown in Fig. S4 (b) and (c), depending on the exact location of M , the boundary can cut two columns of J_2 bonds (as in (b)) or avoid cutting J_2 bonds at all (as in (c)). Numerically, we find that the three choices of M yield distinct values and scaling behavior of the disorder parameter $\langle X_M \rangle$. Only for those regions cutting no J_2 bonds, finite-size scaling analysis converges to the expected result for the $(2+1)d$ O(3) CFT. The issue can be clearly seen from the representative data in Fig. S5. Fig. S5 (a) shows the $|\langle X_M(\theta) \rangle|$ at $\theta = \pi/2$ for $L = 96$ at the QCP of $H_{J_1-J_2}$. Disorder parameters corresponding to three different boundaries as illustrated in Fig. S4 (a), (b) and (c), denoted as odd, even-A and even-B in the figure all show different perimeter dependence. Even-A type boundaries show the largest linear coefficient in the perimeter contribution, which makes sense as this type of boundary cuts the most J_2 bonds. While the perimeter law is non-universal, the dependence on the details of the boundary also manifests in the corner correction, at least in our finite-size analysis. The problem is clearly illustrated in Fig. S5 (b), where $s(\theta)$ extracted from the disorder parameters computed using the three types of boundaries are shown for system size $L = 96$. Here one sees that s for Even-A boundary becomes negative, which violates the positivity constraint at $\theta = \pi$ and is obviously unphysical. We believe that the relatively large perimeter contribution for Even-A boundary data strongly affects the precision of the fitting, since the corner contribution is subleading to the perimeter term. For the other two types of boundaries (Odd and Even-B), now both give positive $s(\theta)$, but the θ dependence is still quite different. We find it is the Even-B type regions that give the correct value of the current central charge of the O(3) CFT, from fitting $s(\theta) \approx \frac{c_J}{(4\pi)^2} \theta^2$. This analysis suggests that to mitigate the finite-size error in the data fitting, one should construct disorder operators on regions which minimize the perimeter contribution. In particular, when there is lattice symmetry breaking induced by “bond” order, the strong bonds should be avoided.

In case of the DQC, although H_{J-Q_3} is translation-invariant, it is already well-known that finite-size analysis of correlations can be tricky due to the domains of VBS formed spontaneously when $Q \geq Q_c$. For disorder operator, boundary dependence similar to those observed in the $J_1 - J_2$ model also shows up in the naive measurements of $\langle X_M \rangle$ at DQC. To minimize the effect of cutting strong bonds due to residual VBS order, we add a small pinning field to the Heisenberg term following the same pattern in the $H_{J_1-J_2}$ model, with $J_1 = J$ and $J_2 = J + \delta/L$. In this way, the VBS can be weakly pinned by the J_2 term but the order vanishes as $L \rightarrow \infty$. With such a setup, we then measure the $\langle X_M \rangle$ with even-B type boundary as in Fig. S4 (c). A comparison of measurements with three different boundaries is given in Fig. S6. We find that this method achieves the most robust convergence of $\langle X_M \rangle$ at DQC, as shown in the main text.

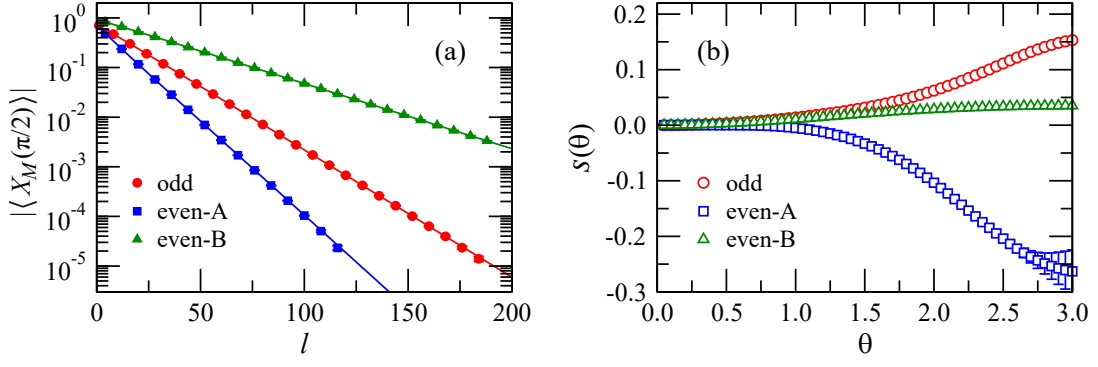


FIG. S5. $|\langle X_M(\theta) \rangle|$ for the $H_{J_1-J_2}$ model, all obtained with $L = 96$: (a) disorder parameter as functions of l at $\theta = \pi/2$, for the three types of the region M . (b) $s(\theta)$ for the three types of the region M , respectively.

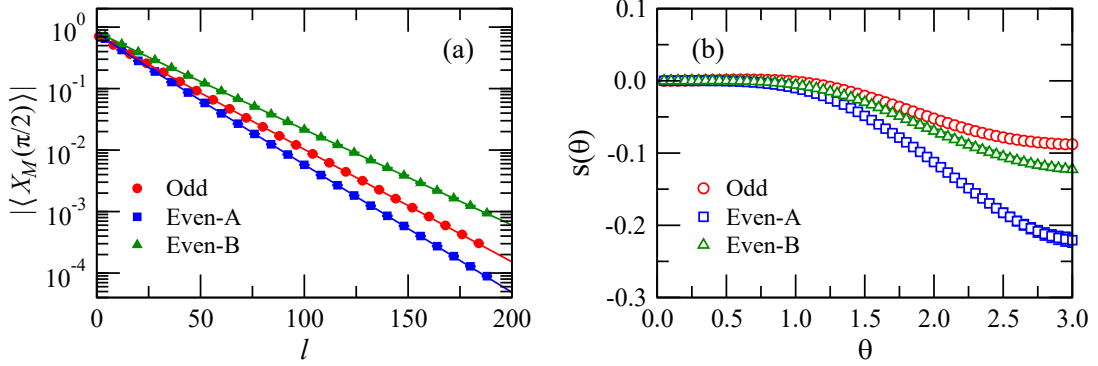


FIG. S6. $|\langle X_M(\theta) \rangle|$ for the H_{J-Q_3} model with a small pinning field, all with $L = 96$: (a) disorder parameter as functions of l for $\theta = \pi/2$ for the three types of the region M , respectively. (b) $s(\theta)$ for the three types of the region M , respectively. It is interesting to note here that all three different types of M lead to negative $s(\theta)$ when θ is close to π .

POSITIVITY CONSTRAINT ON \mathbb{Z}_2 DISORDER PARAMETER

In Ref. [39] it was shown that in a general unitary quantum field theory (QFT), Rényi entropies satisfy the following inequality:

$$\det \left(\left\{ e^{-(n-1)S_n(M_i \cup \bar{M}_j)} \right\}_{i,j=1,\dots,m} \right) \geq 0. \quad (\text{S1})$$

Here $M_i, i = 1, \dots, m$ is a collection of (codimension-1) regions in the half space of positive Euclidean time, and \bar{M}_j is the Euclidean time-reflected regions corresponding to M_j .

We now prove a similar inequality for \mathbb{Z}_2 disorder operator. Suppose that U_g is a \mathbb{Z}_2 symmetry in the QFT (i.e. $U_g^2 = 1$ and therefore U_g is hermitian), which is represented by a topological surface operator in the Euclidean spacetime. The disorder parameter for a region M is then given by the (suitably normalized) path integral with an insertion of an open surface operator X_M , which is just U_g restricted on M . Following Ref. [39], we split the path integral for positive and negative Euclidean time. Consider a family of M_i in the positive Euclidean time half-space, and write ϕ^\pm for fields restricted to positive and negative Euclidean time. We have

$$\begin{aligned} \sum_{i,j} \lambda_i \lambda_j^* \langle X_{M_i \cup \bar{M}_j} \rangle &= \mathcal{N}^{-1} \sum_{i,j} \lambda_i \lambda_j^* \int^{M_i \cup \bar{M}_j} \mathcal{D}\phi e^{-S[\phi]} \\ &= \mathcal{N}^{-1} \int \mathcal{D}\phi_0(\mathbf{x}) \left(\sum_i \lambda_i \int_{\phi^+(0,\mathbf{x})=\phi_0(\mathbf{x})}^{M_i} \mathcal{D}\phi^+ e^{-S[\phi^+]} \right) \left(\sum_j \lambda_j^* \int_{\phi^-(0,\mathbf{x})=\phi_0(\mathbf{x})}^{\bar{M}_j} \mathcal{D}\phi^- e^{-S[\phi^-]} \right). \end{aligned} \quad (\text{S2})$$

Here the subscript M indicates insertions of the corresponding open surface operators in the path integral. Equivalently, one may view the insertion as changing the boundary condition of the fields along the surface M . The normalization factor $\mathcal{N} = \int \mathcal{D}\phi e^{-S[\phi]}$ is just the path integral without any open surface inserted. ϕ_0 is the common value of ϕ^+ and ϕ^- at Euclidean

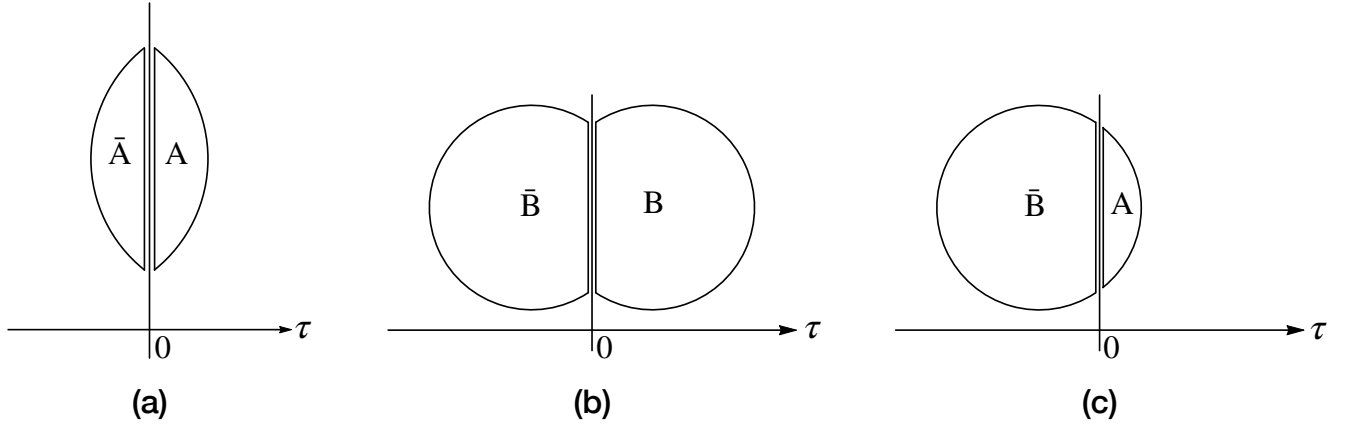


FIG. S7. (a) Regions A and \bar{A} . \bar{A} is the Euclidean time-reflected image of A with respect to $\tau = 0$. The two regions touch each other at the $\tau = 0$ plane, and we take the limit of no separation. Together $A \cup \bar{A}$ has two sharp corners. (b) Regions B and \bar{B} . (c) Regions A and \bar{B} . $A \cup \bar{B}$ has no corners.

time $\tau = 0$. If the action has the time-reflection symmetry $\mathcal{S}[\phi(\tau, \mathbf{x})] = \mathcal{S}[\phi(-\tau, \mathbf{x})]^*$, together with the hermiticity of the inserted operator, a change of variables $\phi(\tau, \mathbf{x}) \rightarrow \phi(-\tau, \mathbf{x})$ in the path integral proves that the two terms in the brackets are complex conjugate of each other, and the result is positive. Since λ_i 's are arbitrary complex numbers, the condition is equivalent to

$$\det \left(\left\{ \langle X_{M_i \cup \bar{M}_j} \rangle \right\}_{i,j=1,\dots,m} \right) \geq 0. \quad (\text{S3})$$

In the following we will write $\langle X_M \rangle = e^{-S(M)}$ (S not to be confused with the entropy or the action \mathcal{S} in the path integral). In a CFT in $(2+1)d$, $S(M)$ should take the following form:

$$S(M) = a_1 |\partial M| - s \ln \frac{l_M}{\delta} + a_0 + O\left(\frac{\delta}{l_M}\right). \quad (\text{S4})$$

Here ∂M denotes the boundary of M , and $|\partial M|$ is the perimeter of the region. l_M is the linear size of M and δ is a short-distance cut-off. s is the sum of universal constants for each sharp corner of the region.

When $m = 2$, denote the two regions by A and B , the inequality reduces to

$$2S(A \cup \bar{B}) \geq S(A \cup \bar{A}) + S(B \cup \bar{B}). \quad (\text{S5})$$

Now we choose the two regions A and B as shown in Fig. S7. The region $A \cup \bar{A}$ has two sharp corners with the same opening angles α , while $B \cup \bar{B}$ has two corners with opening angles $2\pi - \alpha$. It can be easily checked that

$$|\partial(A \cup \bar{A})| + |\partial(B \cup \bar{B})| = 2|\partial(A \cup \bar{B})|, \quad (\text{S6})$$

where $|\partial(V)|$ is the perimeter of the region V . Thus the perimeter terms in S all cancel out. We then note that $A \cup \bar{B}$ has a smooth boundary with no corners. Notice that A and B can be considered to have the same linear size l . So in order for the inequality to hold for arbitrary linear size of the region, generally we must have

$$-2s(\alpha) \ln \frac{l}{\delta} - 2s(2\pi - \alpha) \ln \frac{l}{\delta'} + \text{const.} \leq 0. \quad (\text{S7})$$

It is not difficult to show that $s(\alpha) = s(2\pi - \alpha)$, therefore in order to satisfy Eq. (S7) for arbitrarily large l , $s(\alpha)$ must be positive.

A slight generalization of the argument, with B having opening angle β instead of $2\pi - \alpha$, gives

$$s(\alpha) + s(\beta) \geq 2s\left(\frac{\alpha + \beta}{2}\right). \quad (\text{S8})$$

Together with $s(\alpha = \pi) = 0$ we can see that $s(\alpha)$ is a non-negative, decreasing and convex function of α for $0 \leq \alpha \leq \pi$. Similar conclusions for Rényi entropies were obtained in Ref. [40].